 https://doi.org/10.3311/PPci.20607

Periodica Polytechnica Civil Engineering, 66(4), pp. 1098–1113, 2022

Experimental and Probabilistic Investigations of the Effect of Fly Ash Dosage on Concrete Compressive Strength and Stress-strain Relationship

Truong-Thang Nguyen[1], Viet-Hung Dang[2*]

[1] Department of Concrete Structures, Faculty of Building and Industrial Construction, Hanoi University of Civil Engineering (HUCE), No.55 Giai Phong Rd., Hai Ba Trung Dist., Hanoi, Vietnam
[2] Department of Structural Mechanics, Faculty of Building and Industrial Construction, Hanoi University of Civil Engineering (HUCE), No.55 Giai Phong Rd., Hai Ba Trung Dist., Hanoi, Vietnam
[*] Corresponding author, e-mail: hungdv@huce.edu.vn

Received: 06 June 2022, Accepted: 12 July 2022, Published online: 22 July 2022

Abstract

The effect of fly ash (FA) dosage on concrete's compressive strength and stress-strain relationship is investigated in two steps in this article. First, an experimental program was conducted on concrete mixtures designed with 0% (control batch of 30 MPa mean cylinder compressive strength), 10, 20, 30, and 40% of ordinary Portland cement (OPC) mass replaced by FA, which is taken from a new source in an Asia country. The test results showed that compared to other investigated dosages, concrete using 20% FA/OPC mass-replacement gained the most improvement in the 28-day compressive strength and tensile split strength, as well as the compressive strength development. Second, a probabilistic investigation was conducted using Dropout Neural Network, Bayesian Neural Network, and Gaussian Process models. These artificial intelligence-based models were compared to other models reviewed from the literature, showing relatively good results in terms of the statistical metric R^2, which are 0.92, 0.9, and 0.88, respectively. The three models were tested and validated with a dataset of 1032 experimental results on FAC collected from the literature. When testing with the experimental results obtained in the first step, a good correlation between the predicted values and the experimental results was observed within the confidence interval of (5%, 95%), showing the reliability of the proposed models. Thus, the stress-strain relationship of fly ash concrete can also be investigated in a probabilistic manner. It is proved in this study that among the proposed models, Dropout Neural Network has the best balance between performance and time complexity.

Keywords

fly ash, concrete, strength, stress-strain, probabilistic, machine learning, neural network

1 Introduction

The requirement of harmonization between economic development and environment protection is becoming a worldwide trend nowadays. In recent decades, researchers' special attentions have been paid to the utilization of industrial byproducts, i.e., fly ash, silica fume, blast furnace slag, etc. as alternative sources for building materials, especially for concrete construction. The idea of using fly ash (FA) to partially or fully replace ordinary Portland cement (OPC) as a binder in concrete totally meets the requirement of sustainable construction since it not only reduces the carbon dioxide from the cement manufactory, that occurs worldwide greenhouse effect, but also sufficiently solves the problem of industrial waste materials. At the beginning, FA was mostly utilized as an additive to the admixtures of concrete for the benefits in workability of fresh concrete. Then, replacing various proportions of OPC with an appropriate amount of FA as a binder was found to be efficient to enhance mechanical properties of fly ash concrete (FAC) [1, 2]. The actual FA amount used varies widely depending on the application, mechanical and chemical properties of FA, specification limits, as well as on the geographic location and climate. It is specified by ACI Committee 232.2R-18 that FA can be introduced in concrete either as a separately-batched material or as a component of blended cement with the normal rate of 15 to 35% by mass of total cementitious material [1, 3]. The ACI code also specifies that for fly ash in different types and from various sources, individual study shall also be conducted

Cite this article as: Nguyen, T.-T., Dang, V.-T. "Experimental and Probabilistic Investigations of the Effect of Fly Ash Dosage on Concrete Compressive Strength and Stress-strain Relationship", Periodica Polytechnica Civil Engineering, 66(4), pp. 1098–1113, 2022. https://doi.org/10.3311/PPci.20607

to determine the appropriate percentages of total by-mass cementitious materials of fly ash and other pozzolans. This fact motivated the authors to conduct an experimental study to obtain a new dataset to examine the application ability of a new source of FA from Hongsa thermal power plant (Lao DPR) in concrete industry of the country. The main concern is to investigate the effect of FA/OPC mass-replacement percentage on a number of mechanical properties of FAC including compressive strength, split tensile strength and stress-strain relationship. The replacement percentage was gradually increased from 0% (control batch with 30 MPa cylinder compressive strength), 10, 20, 30, and 40% by mass. The water/binder ratio and the total binder weight in the concrete mixture were both kept constant. The tests were conducted at the Building Construction and Inspection Laboratory LAS-XD 125, Hanoi University of Civil Engineering (HUCE).

Since the late of the 20th century, artificial intelligence approaches have been widely adopted to analyze and predict mechanical properties of concrete [4]. However, these advanced methods have not been commonly applied in the research works performed on the utilization of fly ash from Asian countries recently [5–12]. Meanwhile, Young et al. [13] collected a database of more than 10,000 concrete samples then used the database to train Machine Learning (ML) models for predicting the compressive strength of concrete; the obtained results are reliable with an average error of around 10%. Nguyen et al. [14] investigated Deep Learning architectures to predict the compressive strength of fly ash concrete and found that these models can provide an acceptable error rate of under 20%. Tahwia et al. [15] adopted artificial neural network (ANN) for the prediction of the nonlinear relationship of various fly ash concrete properties at different ages from 3 to 180 days with their ingredients. Besides, other statistical models providing more feature interpretations such as Gaussian Process for Regression, Multivariate Adaptive Regression Spline etc. have been explored by various authors [16, 17]. Ahmad et al. [18] used a number of ML techniques to investigate the compressive strength of fly ash-based geo-polymer concrete, their performances were evaluated and compared via different metrics, showing that the ensemble-based technique achieved the highest performance. A similar conclusion was also confirmed by Amin et al. [19]. Furthermore, the authors pointed out that fly ash and temperature have significant impact on the concrete strength via feature importance study. For non-ensemble learning model, Khursheed et al. [20] found that minimax probability machine regression method could outperform counterparts in predicting the compressive strength at 28 days of fly-ash concrete. Recently, a thorough review about more than 30 ML models for predicting mechanical properties of concrete could be found in [21]. Furthermore, data-driven has been proved to be able to effectively predict the performance of whole 3D structures with numerous elements [22], even with the presence of complicated components such as seismic excitations [23], semi-rigid connections [24]. Among a vast configuration of ANN with various topologies, different possible weight values, some special techniques such as back-propagation or counter propagation [25] are required to learn the most optimal model parameters. Furthermore, depending on unique properties of each investigated structure, some specialized techniques could be derived to improve the performance and stability of ANN models, e.g., data ordering in [26]. Hence, after obtaining self-conducted experimental results, the authors developed three data-driven models using probabilistic approaches including Dropout Neural Network (Dropout-NN), Bayesian Neural Network (Bayesian-NN), and Gaussian Process (GP) models. A fair number of 1032 experimental results collected from literature [27] were incorporated to investigate the effect of FA/OPC replacement percentage on concrete compressive strength and stress-strain relationship.

2 Research significance

The aforementioned reviewed works on using ML models for predicting the compressive strength of fly ash concrete are enumerated in Table 1 [14, 18–20, 28–30].

It can be seen in Table 1 that the novelty of the ML application in this study is the use of probabilistic models, which is capable of not only providing well-predicted results but also estimating how confident the results are through the associated confidence intervals. Such a kind of result is more relevant for experimental data rather than a single point estimation because even with the same ingredients and ratio, one usually still obtains slightly scattered results from different series of experiments.

The analysis results of the three probabilistic models adopted in this study are compared to those of another 27 ML models used in the aforementioned reviewed works. With relatively good analysis results obtained, it is shown that the most favorable FA/OPC mass-replacement percentage in terms of compressive strength is determined by both experimental and probabilistic approaches in this study.Furthermore, the stress-strain relationship of fly ash

Table 1 Summary of reviewed research works

Works	Machine learning model & Type		Fly ash concrete data	Database size
Nguyen et al. [14]	DNN and ResNet-based models	Deterministic	by the authors	335
Ahmad et al. [18]	BR, AR, DT	Deterministic	From literature	154
Amin et al. [19]	DT, SVR, baggin, AdaBoost, RF	Deterministic	From literature	156
Khursheed et al. [20]	MPMR, RVM, GP, ENN and ELM	Deterministic	From literature	112
Sevim et al. [28]	MLR, ANN, PSO-Anfis, GA-Anfis	Deterministic	by the authors	196
Huang et al. [29]	SVR-based models + HLO optimization	Deterministic	From literature	144
Farooq et al. [30]	Ensemble models	Deterministic	From literature	1030
This study	Dropout-NN, Bayesian-NN, GP	Probabilistic	From literature + by the authors	1109 (1032+77)

concrete is also analyzed by probabilistic ML models, whereas most of the previous research works only focused on the concrete strength, which is only the peak point of the curve.

Last but not least, the new test results obtained by the authors on the fly ash taken from a new source also contribute to and enrich the experimental database of mechanical properties of concrete using fly ash from various thermal power plants in Asia and the world. These results show the feasibility of utilizing fly ash in concrete as a sustainable construction material and help developing countries in Asia adapt the worldwide trend of harmonizing economic development and environmental protection with the mean of green construction.

3 Experimental investigations

3.1 Specification of test specimens

The concrete mixture proportions of test specimens are shown in Table 2.

In the table, the control mixture that purely used cement as the binder (0% of FA/OPC) is labeled as MS-30-00, in which the term "MS" stands for "material specimen" and the number "30" is to represent the target mean cylinder compressive strength of the control batch, which is 30 MPa. FA/OPC mass-replacement percentages of 10, 20, 30 and 40% were designed for the remaining mixtures, which can be referred to as MS-30-10, MS-30-20, MS-30-30, and MS-30-40, respectively. It is noted that the total weight of binders (including OPC and FA) and the water/binder (W/B) ratio were both kept constant at 380 kg/m^3 and 0.54, respectively. Besides, due to the difference between the specific gravities of OPC and FA, there was an increment in the total FAC volume when OPC was partially replaced by FA. Then, the corresponding proportions calculated for a cubic meter of FAC are put in the parentheses.

Table 2 Concrete mixture proportion (in kg)

Mixture	Cement	Fly ash	Sand	Gravel	Water
MS-30-0	380	0	760	1140	205
MS-30-10	342 (339.0)	38 (37.7)	760 (753.3)	1140 (1130.2)	205 (203.2)
MS-30-20	304 (298.7)	76 (74.7)	760 (746.8)	1140 (1120.2)	205 (201.4)
MS-30-30	266 (259.1)	114(111.1)	760 (740.3)	1140 (1110.5)	205 (199.7)
MS-30-40	228 (220.2)	152 (146.8)	760 (734.0)	1140 (1101.0)	205 (198.0)

In this study, local OPC with a specific gravity of 3.1 g/cm^3 and the fineness determined following the Blaine method higher than 2800 cm^2/g was used. These properties are all in accordance with ASTM C150/C150M [31].

The chemical composition and physical properties of the particular fly ash used in this study are also listed in Table 3. It was determined by the Blaine method [32] that the FA used in this research had a specific surface area of 2123 cm^2/g. The results were based on the residual amount of 42.4% retained on a 45 μm sieve. The specific gravity of the material was also determined as 1.88 g/cm^3 [32].

In Table 2, the coarse aggregates were gravel produced from local crushed stone having a nominal maximum size of 20 mm. The fine aggregate was also from local natural sand with a maximum particle size of 5 mm. The aggregates' sizes were all within the allowable limits specified in ASTM C33/C33M [33].

Testing on material specimens was conducted at LAS-XD 125, Hanoi University of Civil Engineering (NUCE). Concrete cylinder specimens with 150 mm-diameter and 300 mm-height, as well as 150 mm-cube specimens were prepared for experimental studies according to international and local standards, respectively [34, 35]. Both cylinders and cubes were cast for testing of compressive and tensile strengths as well as the stress-strain relationship of the investigated mixtures. The compressive

Table 3 Properties of fly ash used

Chemical composition	Unit	Value
SiO_2	%	40.54
Al_2O_3	%	29.55
Fe_2O_3	%	4.56
CaO	%	5.58
MgO	%	0.03
Na_2O	%	0.93
K_2O	%	0.32
SO_3	%	0.34
P_4O_{10}	%	0.05
TiO_2	%	0.38
MnO_2	%	0.03
Physical properties		
Specific gravity	g/cm³	1.88
Blaine fineness	cm²/g	2123
% Retained on 45 μm	sieve of No. 325	42.40
Loss on ignition	%	0.69
Water requirement	% of the control	102.00
Strength index at 7 days	% of the control	86.00
Strength index at 28 days	% of the control	93.00

strengths were measured at 7, 14, 28 and 90 days, with every three samples in a test group to calculate the average results. After de-molding at the one-day age, the concrete specimens were cured in large plastic bags at room temperature until being tested.

3.2 Experimental results

3.2.1 Workability of concrete

Fig. 1 shows the workability of fresh concrete mixtures in terms of slump values. It can be seen that although the control mixtures MS-30-00 (OPC) and MS-30-10 (10% FAC) had equal slumps, there is a general trend that the slump increases with an increment in the FA/OPC replacement percentage. This is because most FA particles are spherical in shape with various sizes and have good dispersion, whereas cement particles have irregular polygonal shapes. As a result, FAC mixtures have a lower water requirement than the control concrete mixture.

The unit weights were measured from all the concrete mixtures at 7-day and 20-day ages as shown in Fig. 2. It can be seen in Fig. 2 that an increase in FA/OPC mass-replacement percentage leads to a decrease in concrete unit weight. At 7-day age, there is a 6.35% reduction in unit weight between OPC concrete (2524 kg/m³) and 40% FAC (2364 kg/m³). Likewise, the corresponding concrete unit weight at the 20-day age was reduced from 2499 to 2345 kg/m³, i.e., with a reduction of 6.16%. The reduction in the unit weight of FAC is due to the low specific gravity of FA compared to OPC. The control mixtures (0% FA/OPC) had the highest water loss, whereas the 40% FAC mixture had the lowest value.

In conclusion, it can be seen from Figs. 1 and 2 that using FA helps concrete gain better workability in terms of the concrete slump and the rate of hydration reaction.

3.2.2 Concrete strengths

The 28-day cylinder compressive strength measured from testing is shown in Fig. 3. It is noticed from the figure that the 20% FAC (MS-30-20) performed the maximum cylinder compressive strength, which is 31.1 MPa, compared to the remaining replacement ratio and is even a bit higher than those of the original OPC concrete, which is

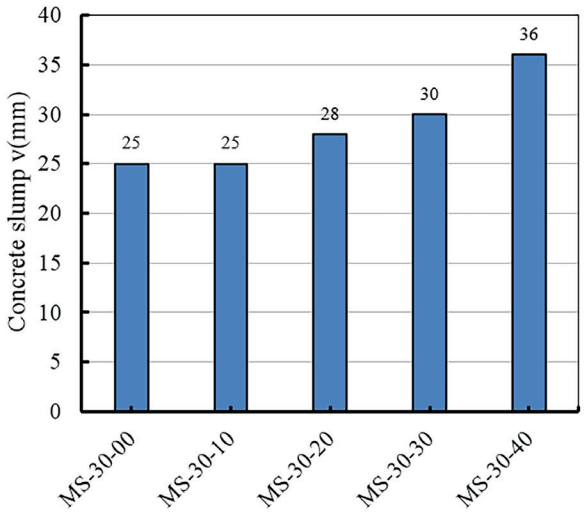

Fig. 1 Measured slump of fresh concrete

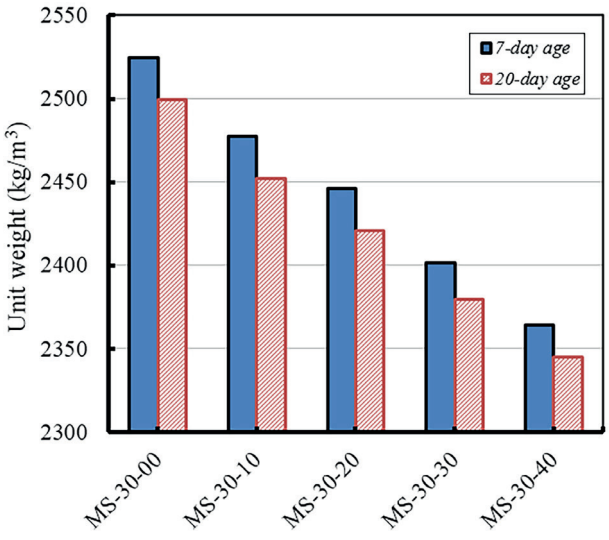

Fig. 2 Measured concrete unit weight

30.44 MPa. Meanwhile, the 30% (MS-30-20) and 40% (MS-30-40) FAC specimens had relatively low values of 22.20 and 20.41 MPa, corresponding to the respective considerable reductions of 27.1% and 33.0% from that of the control OPC concrete.

A similar trend can also be observed from the test results on tensile split strength shown in Fig. 4. It is shown that the 20% FAC test value of 3.07 MPa is the maximum tensile split strength, followed by those of 10% FAC and OPC concrete, which are 3.05 and 2.78 MPa, respectively. The tensile split strength values of the 40% and 30% FAC specimens were again the lowest values obtained from the experiments.

The development of compressive strength at 7, 14, 28, 56, and 90-day ages obtained from testing on 150 × 300 mm cylinder specimens are shown in Fig. 5.

It can be seen in Fig. 5 that all the FAC concrete had lower compressive strength than the control OPC concrete before the age of 7 days. However, from the age of 14 days, the 10% and 20% FAC had the higher values. From 28-day onward, the 20% FAC gained the maximum compressive strength with the highest development curve compared to the others. Besides, a slight improvement in strength with age can also be observed for 20% FAC.

3.2.3 Stress-strain curve

Testing to obtain the stress-strain curve of FAC concrete was conducted in accordance with ASTM C469 [36] on 150 mm by 300 mm cylinder samples. In principle, a displacement-controlled compression machine should be used in order to capture the post-peak part of the curve since the cylinder of the hydraulic jack can be set to move downward to the concrete specimen with an instant displacement rate to maintain the compression pressure on the specimen even when the peak of the stress-strain curve is reached. A displacement limit can also be set to ensure the safety of the whole system when the specimen is totally damaged. This is impossible when the load-controlled compression machine is used in the test because of the loss of attachment between the machine and the specimen after the peak, leading to the loss of compressive pressure on the specimen. On the other hand, continuing to increase the compression load without any limitation at this post-peak stage may lead to a dangerous situation for the apparatus in the testing system when the specimens are totally failed.

However, since there was a lack of displacement-controlled compression machine associated with an actuator at the Building Construction and Inspection Laboratory

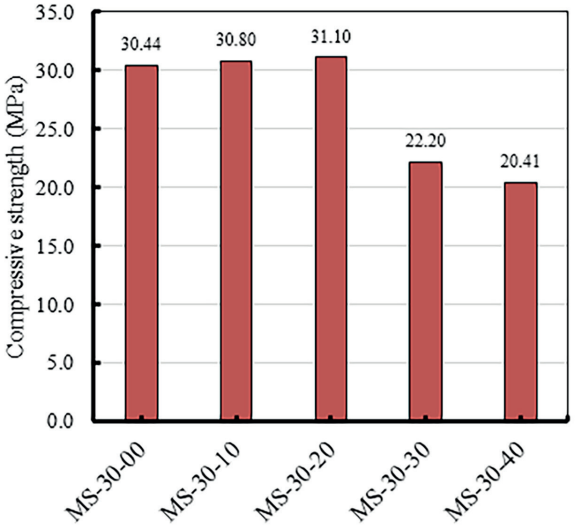

Fig. 3 Experimental results of compressive strength

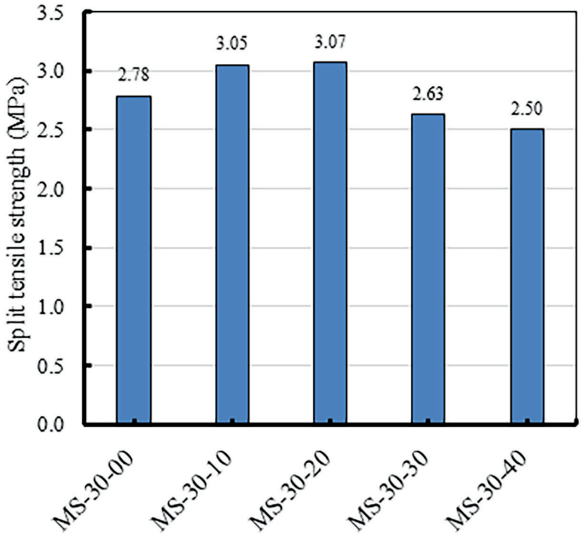

Fig. 4 Experimental results of tensile split strength

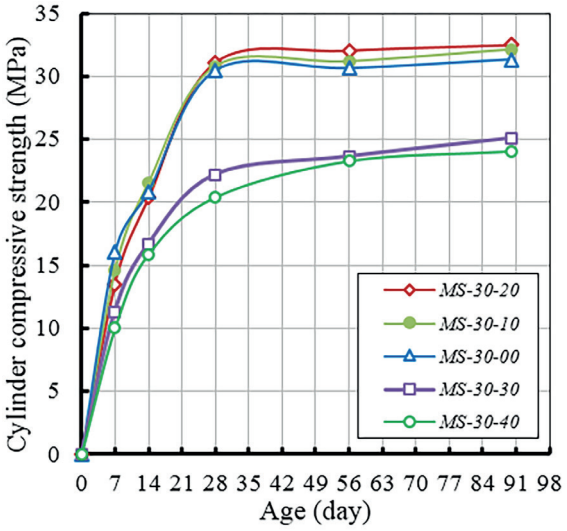

Fig. 5 Experimental results of strength development

LAS-XD 125, Hanoi University of Civil Engineering (NUCE), an improvement solution was proposed to overcome this difficulty as follows:

- A specimen from the same batch shall be tested in advance just to approximately determine the stress value at peak. The load-controlled machine shall be operated by a well-qualified and experienced technician so that he could purposely adjust the loading rate from 300 kPa/s during the first stage from 0–40% of the maximum stress down to 200 kPa/s during the second stage of 40–90%, and then to 50–100 kPa/s when a level of 90% of the peak stress is reached till the end of the test. This is to obtain the stress-strain curve not only to the peak but also to the remaining post-peak part.
- All the LVDTs shall be installed to the steel plate fixed to the cylinder of the hydraulic jack, with a measurement length of 300 mm (equals to the specimen height) instead of being installed directly to the specimen (with a measurement length of 150 mm) or instead of attaching the concrete strain-gauges to the concrete surface. This is to avoid all the disturbances occurred by cracks on the surfaces of the specimens, especially when the peak of the stress-strain curve is reached. Hence, strain data can still be measured for the post-peak behavior;
- The test shall be stopped when the strain values reach around 4×10^{-3} mm/mm or severe cracks occur and the specimens are about to break, whichever comes sooner.

By doing so, the whole post-peak behavior may not be fully reflected but at least a number of individual points could be captured. This is the best of the authors' efforts to overcome the difficulty of the laboratory conditions in an Asian developing country like Vietnam.

It is shown in Fig. 6 that the compression machine, LVDTs, load cell located between the compression machine and the column specimen were all connected to a TDS-560 data-logger and a computer to record all the corresponding test data in a 2-second interval.

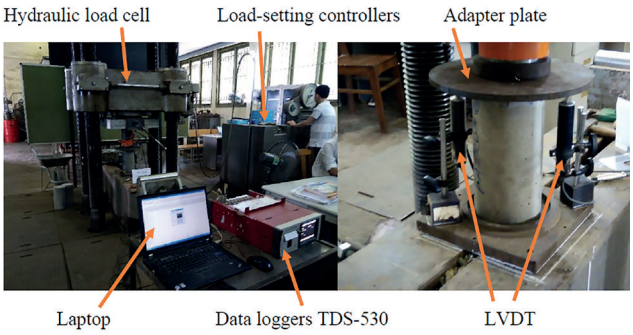

Fig. 6 Experimental setup

The stress-strain curves of FAC specimens measured from the tests are shown in Fig. 7.

A number of observations can be made from Fig. 7 as follows: (i) For 10% and 20% FAC, there is no significant change in compressive strength compared to that of OPC concrete; (ii) For 20% FAC, there is a certain increment in strain value at peak compared to that of OPC concrete, corresponding to a reduction in the stiffness of the material; and (iii) The values of ultimate strains of 0, 10 and 20% FAC are all from 0.30 to 0.40%.

4 Machine learning models for assessing mechanical properties of FAC

Together with the experimental results obtained by the authors, test results on FAC are collected from literature [27] owing to two reasons: (i) Their features, including cement, water, fine and coarse aggregate, fly ash, and curing days, are similar to the FAC tested in this study; and (ii) A total number of 1032 samples is large enough to train a machine learning model. Specifically, histograms of FAC components from the data are illustrated in Fig. 8. Hence, it is useful to develop a data-driven model for predicting FAC compressive strength based on their main ingredients.

On the other hand, the test data obtained by the authors in this experimental study are illustrated via the histograms in Fig. 9.

It is shown in Fig. 9 that the input features, including water, stone, and sand, remain unchanged while cement, fly ash replacement, and ages are varied. The training process and the testing step are completely disjointed, they

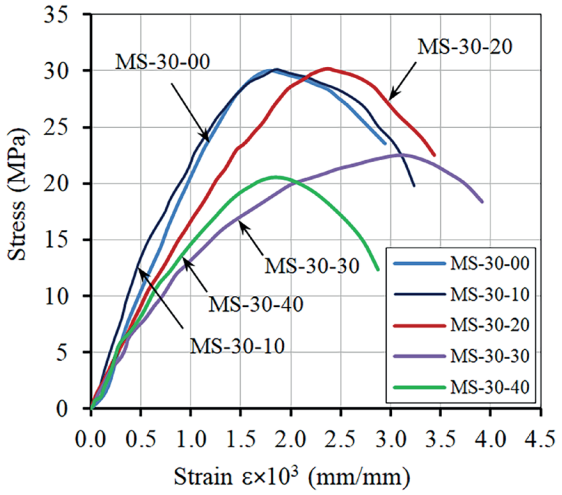

Fig. 7 Experimental results on stress-strain relationship

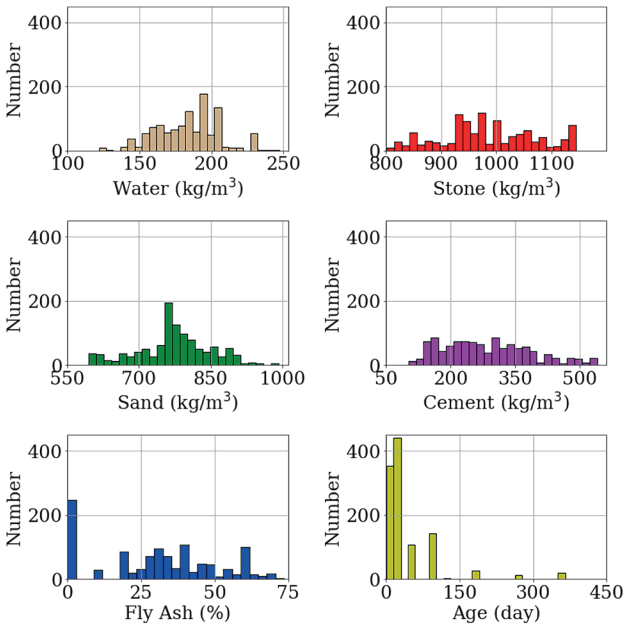

Fig. 8 Histogram of components of FAC collected from literature [16]

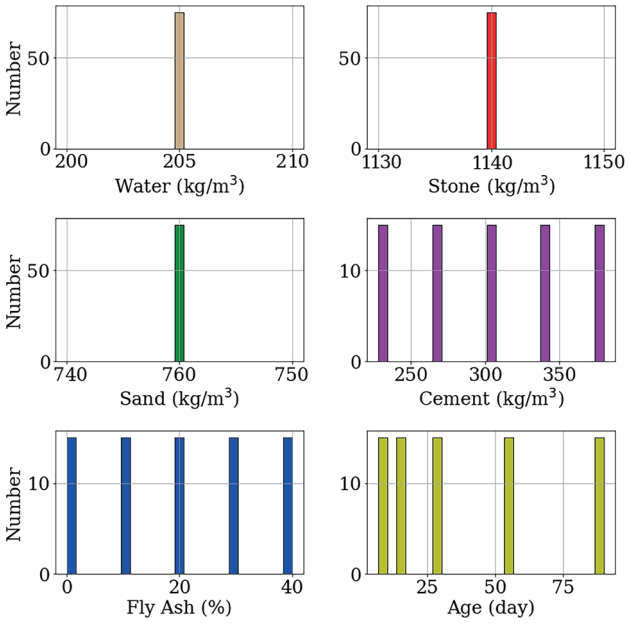

Fig. 9 Histogram of components of FAC from the experiment

use two different databases. However, values of input features of testing data fall within the corresponding ranges of the training and validation data. Thus, one expects that a properly trained model could approximate the compressive strength to some extent.

Furthermore, the uncertainty of the predicted results is also desirable because concrete is an inherently heterogeneous material. Additionally, there are inevitable noise or errors during experiments. Thus, with the same mixture proportions, one can obtain different compression strengths for different experimental series. To this end, three artificial intelligence models, including two neural network-based models, i.e., Dropout Neural Network [37], Bayesian Neural Network [38], and another machine learning model, namely, Gaussian Process [39], are used for probabilistic investigation in this study.

4.1 Conventional Neural Network (ANN)

Mimicking the information flow in the brain where data are processed via a complex system of neurons connected together, a neural network consists of multiple layers, each layer comprises a various number of neurons, forming a nonlinear mapping from input data to output results as shown in Fig. 10(a). Formally, such a nonlinear mapping can be described as follows:

$$Y = F(\boldsymbol{X}|\boldsymbol{W}) = f_L(\ldots(f_2(f_1(\boldsymbol{X}|\boldsymbol{W}_1)|\boldsymbol{W}_2)\ldots\boldsymbol{W}_L), \quad (1)$$

where L is the total number of layers, $\boldsymbol{W}$ is the matrix of the network's parameters to be determined, $\boldsymbol{X}$ and $\boldsymbol{Y}$ stand for input and output vectors, respectively.

The connection between two consecutive layers l-1 and l is performed by aggregating a linear matrix-vector multiplication and a nonlinear activation function as follows:

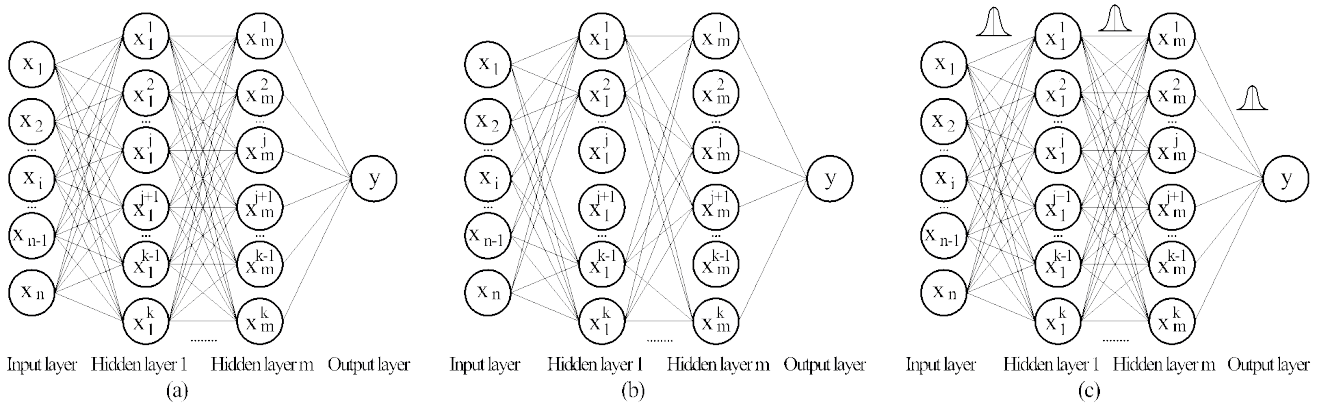

Fig. 10 Architectures of a) Artificial Neural Networks b) Dropout Neural Networks c) Bayesian Neural Networks

$$\boldsymbol{X}_{l+1} = f_l\left(\boldsymbol{X}_l|\boldsymbol{W}_l\right) = h\left(\boldsymbol{W}_l \times \boldsymbol{X}_l + \boldsymbol{b}_l\right), \quad (2)$$

where $l = 1,2,\ldots,L-1$, $\boldsymbol{X}_l$ and $\boldsymbol{X}_{l+1}$ are vector values of layer l and $l+1$, $\boldsymbol{W}_l$ and $\boldsymbol{b}_l$ are weight matrix and bias vector at layer l and h denotes a user-defined nonlinear activation function.

In this study, one adopts the Rectified Linear Unit (ReLU) function for hidden layers, as commonly adopted in the literature. The network parameters $\boldsymbol{W}$ are determined in a supervised manner as follows: at first, one needs to label the FA data, i.e., giving a set of FAC ingredients, then outputs of interest are defined, e.g., the compressive strength. After that, the database is divided into two non-overlapping groups, namely training, and validation datasets. Afterward, the network's weights $\boldsymbol{W}$ are iteratively updated using an optimization algorithm to minimize the deviation between prediction values and actual values. The training process terminates when the error level is sufficiently small, or the number of iterations attains a predefined limit.

4.2 Dropout Neural Network (Dropout-NN)

It is well-known that training a neural network with multiple hidden layers requires a significant amount of appropriate data. Otherwise, if data is limited, the over-fitting problem likely occurs, which means the network performs satisfactorily on training data but produces poor results on unseen testing data. To mitigate this obstacle, the Dropout mechanism is adopted with the main idea that any neuron in the network can be omitted randomly with a predefined probability p. Thus, the resulting network will not be over-relied on any specific nodes (Fig. 10(b)). Dropout Neural Network (Dropout-NN) can be regarded as an ensemble of smaller networks so that it can provide non-optimal but satisfied prediction accuracy with different data, rather than being best-fitted for one particular dataset. Furthermore, Dropout-NN is able to provide statistical estimates such as mean values and standard deviations or confidence intervals rather than a deterministic value of quantities of interest. In this way, one is able not only to obtain predicted results but also to assess how confident results are.

Mathematically, the mechanism of the dropout technique is described in detail as follows. Considering a node j in layer l, its state of presence or absence is independently sampled from a Bernoulli distribution with a predefined probability , as below:

$$r_j^l \sim \text{Bernoulli}\left(p\right), \quad (3)$$

where r_j^l is a binary variable, 0 is to be dropped out, while 1 is to be activated. For the value of Dropout probability p, one adopts the value 0.5 as recommended in [40]. Then the input vector for layer of the network is updated by:

$$\widetilde{\boldsymbol{X}_l} = \boldsymbol{X}_l \otimes r_l, \quad (4)$$

where $\otimes$ denotes the element-wise product, $\boldsymbol{X}_l$ and $\tilde{\boldsymbol{X}}_l$ are the input values for layer l of the original plain network and the dropout network, respectively.

Next, Eq. (2) is rewritten as below:

$$f_l\left(\boldsymbol{X}_l|\boldsymbol{W}_l\right) = h\left(\boldsymbol{W}_l \times \widetilde{\boldsymbol{X}_l} + \boldsymbol{b}_l\right). \quad (5)$$

The described process is analogously applied to every layer in the network except for the output layer. Afterward, the network is trained by performing a number of iterations of forward-pass for calculating output results and deviation and backward-pass to update the weight values $\boldsymbol{W}$. It is noted that at each training iteration, different nodes are eliminated with a probability p, forming different thinner variants of the original plain architecture. In this study, Dropout-NN is constructed by the authors with the help of the deep learning Pytorch [41].

4.3 Bayesian Neural Network (Bayesian-NN)

Bayesian Neural Network (Bayesian-NN) is a Bayesian approach-based deep learning model where network parameters $\boldsymbol{W}$ of a neural network shown in Fig. 10(c) are characterized by their distributions instead of an optimal set of values. The prior distribution of $\boldsymbol{W}$ can be initialized with one of the popular distributions such as uniform or Gaussian ones. Afterward, the training process is carried out to discover the posterior distribution $p(\boldsymbol{W}|D)$ given a dataset ($\boldsymbol{X}$, $\boldsymbol{Y}$). Each weight of Bayesian-NN requires two parameters, i.e., its mean value and variation instead of only one estimated value. The mathematical expression of the weight matrix is re-written as below:

$$\boldsymbol{W} = \boldsymbol{\mu} + \boldsymbol{\sigma} \times \in \text{ with } \in \sim \mathcal{N}\left(0, \boldsymbol{I}\right), \quad (6)$$

where $\boldsymbol{\mu}$, $\boldsymbol{\sigma}$ denote means and standard deviations of $\boldsymbol{W}$, $\boldsymbol{I}$ is the unity matrix. The metric for measuring the performance of the Bayesian-NN is the Kullback-Leibler divergence (KL) expressed as follows:

$$KL(q(\boldsymbol{W} \mid \boldsymbol{\mu},\boldsymbol{\sigma}) \,||\, p\left(\boldsymbol{W}|D\right)) = E_{q(\boldsymbol{W}|\boldsymbol{\mu},\boldsymbol{\sigma})} \log \frac{q\left(\boldsymbol{W}|\boldsymbol{\mu},\boldsymbol{\sigma}\right)}{p\left(\boldsymbol{W}|D\right)}. \quad (7)$$

The implementation of the Bayesian-NN is realized with the help of the probabilistic library Pyro [42] written in Python and supported by the machine learning library

Pytorch. Here, the Bayesian-NN has an architecture of 6/32/32/1, with the prior distribution of the weights being Gaussian distribution with zero mean and unit variance.

4.4 Gaussian Process (GP)

Gaussian Process, also known as the Kriging method, is a Bayesian approach-based machine learning model for probabilistic regression problems, which has been applied in multiple domains such as high-performance concrete, structural reliability, and so on. The core idea of GP is that the closer in space the input data, the more correlated the outputs of the model. Here, GP serves to derive the plausible posterior probability of the compression strength based on the FAC ingredients and training data. Formally, a GP model is a stochastic process which can be fully specified by its mean function $\psi(\boldsymbol{X}) = E[\boldsymbol{Y}(\boldsymbol{X})]$ and its covariance function $C(\boldsymbol{X}, \boldsymbol{X}') = E[(\boldsymbol{Y}(\boldsymbol{X}) - \psi(\boldsymbol{X}))(\boldsymbol{Y}(\boldsymbol{X}') - \psi(\boldsymbol{X}'))]$. Training data consists of n pairs of inputs and targets $\{(\boldsymbol{X}_i, \boldsymbol{Y}_i), i = 1,\ldots,n\}$. Then, let $\boldsymbol{K}$ be the covariance matrix for the training data $k_{ij} = C(\boldsymbol{X}_i, \boldsymbol{Y}_i)$, and $\boldsymbol{k}(x)$ is the covariance vector of a test case with training data. Then, the predictive distribution with its mean and variance can be calculated as follows:

$$\begin{aligned} &\hat{y}(\boldsymbol{X}) = \boldsymbol{k}^T \times \boldsymbol{K}^{-1} \times \boldsymbol{Y}, \\ &\sigma_{\hat{y}}^2(\boldsymbol{X}) = C(\boldsymbol{X},\boldsymbol{X}) - \boldsymbol{k}^T \times \boldsymbol{K}^{-1} \times \boldsymbol{k}. \end{aligned} \tag{8}$$

On the other aspect, one of the most popular choices of covariance functions is squared exponential kernel, namely, Gaussian kernel as below:

$$\boldsymbol{K}(\boldsymbol{X}_i, \boldsymbol{X}_j) = \sigma_0^2 exp\left[-\frac{1}{2}\left(\frac{\boldsymbol{X}_i - \boldsymbol{X}_j}{\lambda} \right)^2 \right], \tag{9}$$

where $x_l^{(i)}, x_l^{(j)}$ are component l of $\boldsymbol{X}_i, \boldsymbol{X}_j$, respectively; λ, σ_0 are hyperparameters to be determined through the training process.

Lastly, the log-marginal-likelihood (LML) function is used as the loss function for measuring the deviation between predicted values and true values.

$$\begin{aligned} &\log\left(p(\boldsymbol{Y}|\boldsymbol{X})\right) = \log\left(\mathcal{N}(\boldsymbol{Y}|0,\boldsymbol{K})\right) = \\ &-\frac{1}{2}\boldsymbol{Y}^T\boldsymbol{K}^{-1}\boldsymbol{Y} - \frac{1}{2}\log|\boldsymbol{K}| - \frac{N}{2}log(2\pi), \end{aligned} \tag{10}$$

where $p(\boldsymbol{Y}|\boldsymbol{X}) = \mathcal{N}(\boldsymbol{Y}|0,\boldsymbol{K})$ is the Gaussian-type likelihood function.

In this study, the implementation of the GP is realized with the aid of the library Gpytorch [43] which is also based on the machine learning library Pytorch.

4.5 Computation results and discussions

4.5.1 Training machine learning models for predicting compressive strength of FAC

In order to train the machine learning models for predicting the compressive strength of FAC based on its components and curing days, the FAC dataset provided by Yeh [27] is employed. Generally, the data are split into two non-overlapping subsets, i.e., training and validation, with a ratio of 80/20. Finally, the model is tested with the experimental data presented in the previous section, which are completely unseen by the model in the training process. The typical training process settings are set as follows: (i) Adam optimizer with an initial learning rate of 10^{-4}, divided by 2.0 when the validation loss does not decrease; (ii) standard normalization used to suppress the scale difference of input variables; and (iii) Kaiming initialization method is adopted for initializing weights' values with zero-center Gaussian distributions. Table 4 summarizes the key parameters of ML models. For Bayesian-NN, the parameters are the number of hidden layers, and the number of neurons per hidden layer, learning rate. For Dropout-NN, there is the percentage of dropout in addition to those mentioned above, and for GP, the parameters are the kernel function for the covariance of GP and the prior mean of GP, which is calculated as the mean of training data. In some studies, GP is referred to as a non-parametric model because the model is mainly determined from data rather than using a set of parameters predefined by users.

On the other aspect, to select an adequate neural network architecture including the number of hidden layers and the number of neurons, the simple yet effective Grid Search technique is utilized. The number of hidden layers varies in the range of (1, 2, 3, 4, 5) while the number of neurons is selected from the range of (8, 16, 32, 64, 128, 256, 512). For simplicity, one utilized the same number of neurons for all hidden layers. Next, each candidate configuration is trained with the same training process mentioned previously. The Grid Search algorithm simply tries all pairs of these two hyper-parameters and then selects the configuration with the lowest loss function on validation data which is the mean squared error expressed as below:

Table 4 Key parameters of machine learning models

Dropout-NN	Bayesian-NN	GP
Layers 6/64/64/1	Layers 6/32/32/1	squared exponential kernel
KL loss	MSE loss	LML loss
l_r = 1E-4	l_r = 1E-4	
p = 0.5	prior distribution of weights $\mathcal{N}(0,I)$	

$$MSE = \frac{1}{N}\sum_{i=1}^{N}\left(Y_i - \hat{Y}_i\right)^2, \tag{11}$$

where N is the number of training data, and $\hat{Y}$ are predicted values. The above procedure is carried out in an automatic fashion with the help of the hyperparameter optimization library Optuna [44]. Neural architecture search results show that the top-3 configurations are: (i) 4 hidden layers of 128 neurons; (ii) 1 layer with 512 neurons, and (iii) 2 layers with 32 neurons, as enumerated in Table 5.

However, it can be seen that the third configuration is significantly less complex than the other, providing a better balance between model performance and model complexity. Specifically, it has about 150 times less parameters to determine than the 6/256/256/256/256/1 architecture (1313 vs. 199425) which achieves the lowest MSE error. Moreover, when adapting ANN for probabilistic models such as Bayesian-NN and Dropout-NN, the number of parameters will be considerably increased due to their specialized requirements, e.g., for Bayesian-NN, the number of parameters will be double since each neuron will have two parameters, i.e., mean and standard deviation.

Table 5 Neural architecture search results

No	Number of layers	Number of neurons	Number of parameters	MSE
1	4	256	199425	0.311
2	1	512	4097	0.313
3	2	32	1313	0.317
4	2	64	4673	0.323
5	3	64	8833	0.328
6	3	256	133633	0.332
7	3	128	34049	0.333
8	2	256	67841	0.333
9	1	64	513	0.335
10	2	128	17537	0.340

Thus, one selects the 6/32/32/1 network architect as the base model for this study, i.e., an input layer with six neurons, two hidden layers with 32 neurons and 1-neuron output for concrete compression strength. More specifically, the input features are fly ash replacement measured in percentage, concrete age in days, and cement, stone, sand, and water, all measured in unit weight (kg/m^3). Meanwhile, the output of interest is the compressive strength measured in MPa. Since these features are of different physical natures and of different scales, thus the data are preprocessed by using the Min-Max Scaler technique to scale all features to the range of (0,1). For Dropout-NN, because one utilizes a dropout rate p of 50%; thus, the number of neurons of hidden layers is doubled to 64.

Fig. 11 displays the training curves for the three probabilistic methods. It is noted though the loss functions are not the same, one still can compare the convergence behavior based on their trends. The learning curve of Dropout-NN decreases rapidly for the first 2000 iterations, followed by the gradual decrease of the loss function. The final model is obtained after 10000 iterations. A similar trend is observed for Bayesian-NN, though its learning curve is more fluctuated. In addition, the training time of Bayesian-NN is nearly double that of Dropout-NN (56 minutes vs. 26 minutes). While for GP, it quickly achieves the best value after around 100 iterations, but afterward, the loss function increases and does not decrease again even with more iterations. The total training time of GP is very fast, i.e., 6 minutes. These results are as expected because the machine learning model usually has a faster convergence rate than those of deep learning models.

The predicted results of the final models are shown in Fig. 12, in which each scattered black point has X and Y coordinates corresponding to experimental strength and the predicted value from the trained models. In addition, the solid red line indicates the ideal case where the

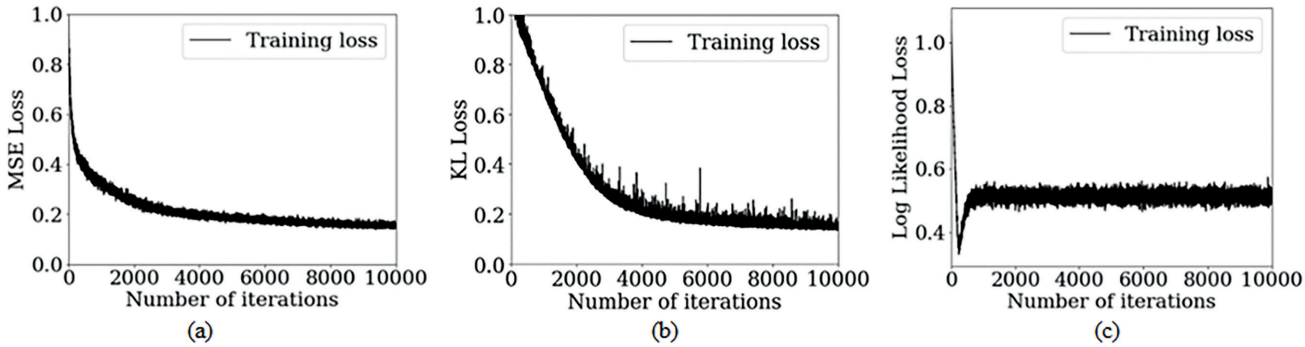

Fig. 11 Training curves for a) Dropout Neural Network b) Bayesian Neural Network c) Gaussian Process

predicted values are exactly equal to the experimental ones, whereas the shaded area refers to the 90% confidence interval (CI) of (5%, 95%), i.e., there is 90% probability that this area will contain actual experimental data. To create the CI, one repeats the prediction 100 times, then derives the mean, 5% and 95% quantile values. Scatter points presented in the figure are random examples obtained from these 100 calculations.

Obviously, with training and validation data, the machine learning models are able to predict the compressive strength of FAC with satisfactory accuracy, as most of the points lie around the ideal 45-degree line. However, for some points relating to very high-performance concretes with a strength of more than 60 MPa, the discrepancy is more pronounced, and the confidence interval is also widened. It is suggested that to improve model performance for high-performance concrete, one should take into account some additional additives as the input features of the machine learning model. On the other hand, when testing with this study's experimental data, a good correlation between the predicted and the experimental values can be observed, as illustrated in Fig. 12 where data points lie close to the ideal 45-degree line. These results confirm the credibility of the proposed probabilistic machine learning models. It is also noted in Fig. 12 that the first row presents results on training data, the second and the third rows are for validation and testing data, respectively.

When comparing the probabilistic models together, the CI of GP is larger than those of Dropout-NN and Bayesian-NN, especially with samples ranging from 0 to 40 MPa on validation data, and around 30 MPa strength of the authors' testing data. In contrast, the Dropout-NN provides the least uncertain results, as its CI area is the smallest but still able to cover almost data points. Thus, in this study, the Dropout-NN yields better performance than the counterparts.

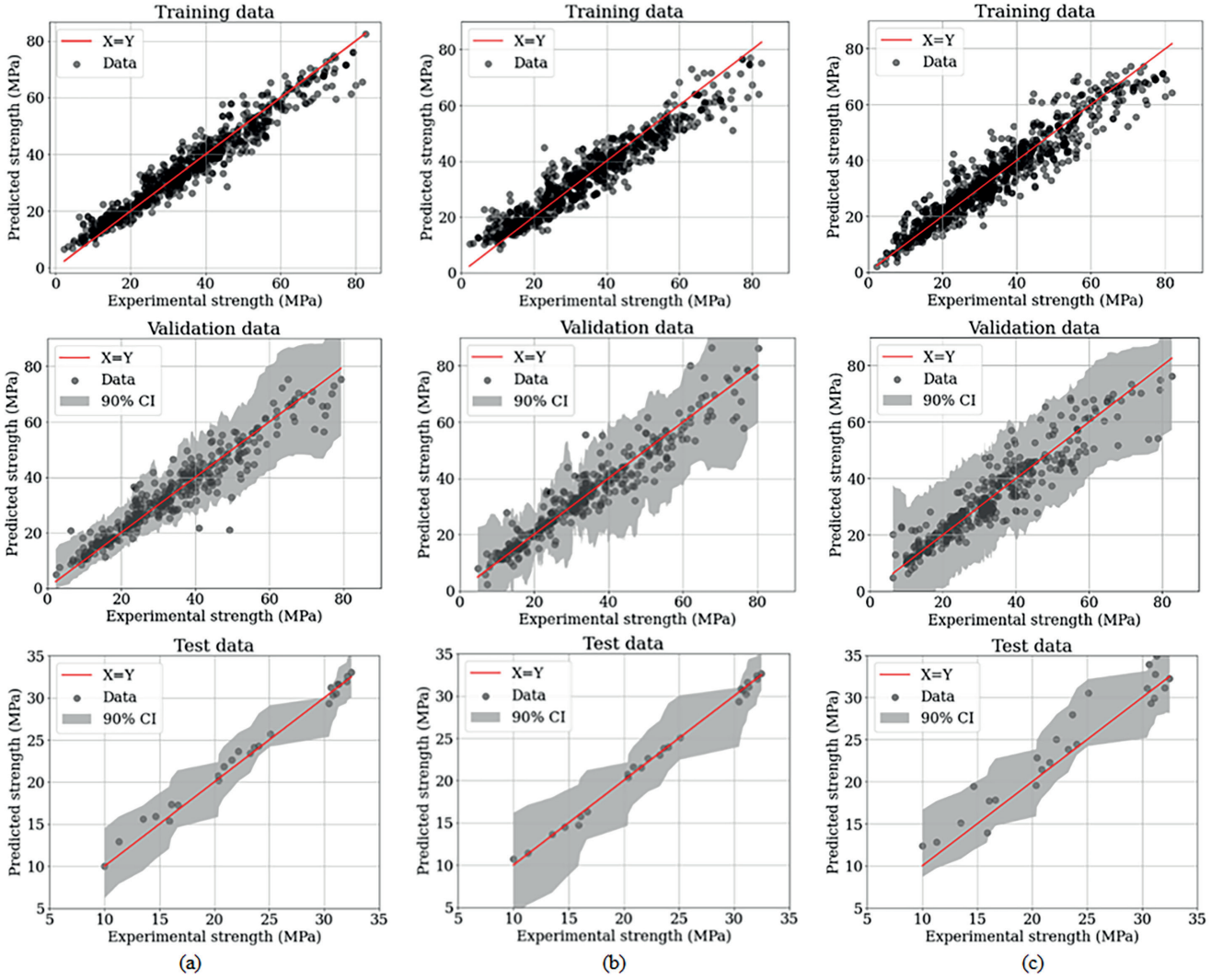

Fig. 12 Prediction results of concrete compressive strength obtained from a) Dropout-NN model b) Bayesian-NN model c) GP model

In addition, Fig. 13 compares the performance of thirty ML models in predicting the concrete compressive strength including three investigated probabilistic models and others in the literature. The model performances are reported using the common statistical metric R^2. It can be seen that linear regression models and some statistic-based ones provide relatively low R^2 results, which means the calculation of compressive strength using FAC components is a non-linear regression problem. The probabilistic models investigated in this study can also achieve relatively accurate results of 0.92, 0.90, and 0.88 for Dropout-NN, Bayesian-NN and GP, respectively. It is noted that though these models do not outperform ensemble-based models, their appealing property is that they can provide the associated uncertainty estimation, as demonstrated above.

Besides, a sensitivity analysis is conducted to estimate the impact of investigated FAC components on the compressive strength prediction. The contribution of each component is calculated via the following equation [18]:

$$\Delta f_i = f_{max}\left(X_i\right) - f_{min}\left(X_i\right), \tag{12}$$

where $f_{max}(X_i)$ and $f_{min}(X_i)$ are maximum and minimum values of compressive strength obtained by models using only i^{th} FAC components while setting other components to their mean values, respectively. Δf_i denotes the contribution score. Furthermore, these contribution scores can be rewritten under the form of relative values measured in percentage as below:

$$C_i = \frac{\Delta f_i}{\sum_1^n \Delta f}. \tag{13}$$

Fig. 14 presents sensitivity results obtained by the three proposed probabilistic models, showing that cement has the largest influence on the compressive strength, followed by concrete age and water. The fly-ash replacement has also noticeable effects on the concrete strength, more pronounced than those of sand and stone. It can also be observed that the neural network-based models assign more distinguishable weights to FAC components than the machine learning Gaussian Process model; thus, the differences between their contribution scores are clearer.

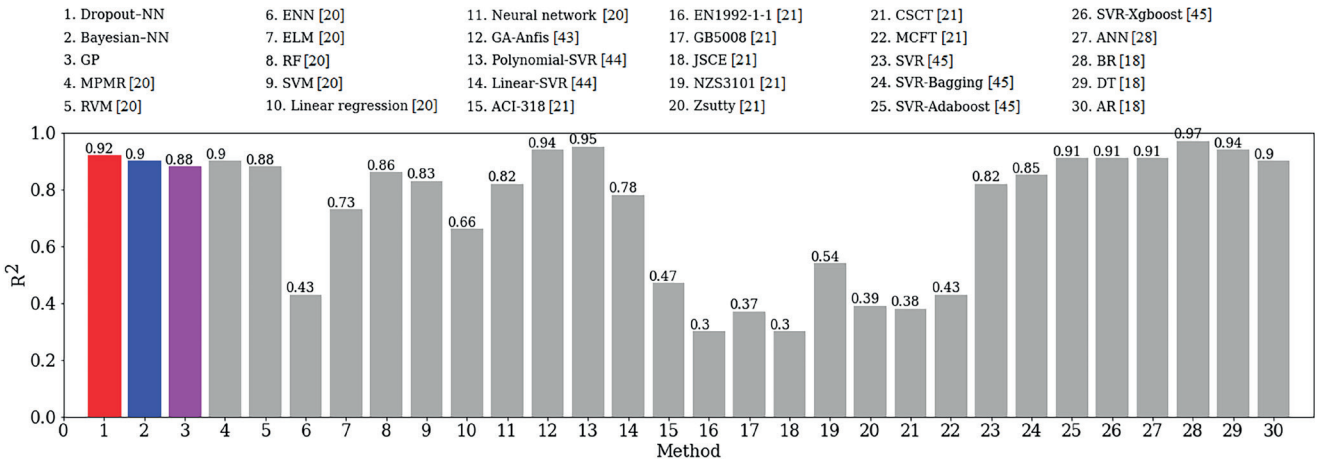

Fig. 13 Comparison of ML models in statistical metric R^2

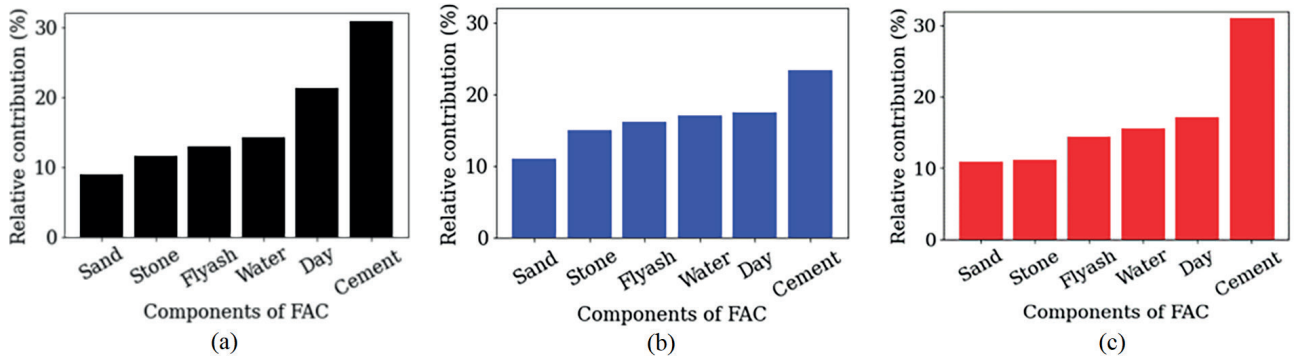

Fig. 14 Sensitivity study results obtained from a) Dropout-NN model b) Bayesian-NN model c) GP model

4.5.2 Probabilistic model for predicting stress-strain curves of FAC

Another application of the probabilistic models proposed in this study is to predict the stress-strain curves of FAC at 28-day age. For this purpose, the architectures of the probabilistic models are the same in Table 5, the output under investigation is stress in MPa, while the input features are water, stone, sand, cement, fly ash replacement, and strain (instead of concrete ages as the previous subsection). The data used to train and validate the probabilistic model are experimental data presented in the previous section with a total of 551 data points, divided into training and validation datasets with a ratio of 80:20. The results for five FA/OPC replacement percentages, namely, 0, 10, 20, 30, and 40% obtained from Dropout-NN, Bayesian-NN and Gaussian Process models are shown in Figs. 15, 16 and 17, respectively.

It is shown in Figs. 15, 16 and 17 that, generally, the probabilistic models can adequately capture the behavior of fly ash concrete from the initial elastic stage to the plastic hardening stage and to softening stage. In addition, the uncertainty will increase with increasing strain for all replacement percentages, for example, using the Dropout-NN model with 20% FA, the 90%-CI around 0.002 strain is nearly 5.0 MPa, which is double that around 0.001 strain (2.0 MPa). The results also suggest that there are more uncertainties with 30 and 40% replacement than those with replacement of 20% or less. Similar trends are also obtained when the Bayesian-NN and GP models are used for the analysis. It can also be seen in the figures that all the three models could provide the results with the same trend and properties as discussed above. However, the CI of the GP model is larger than those of the Dropout-NN

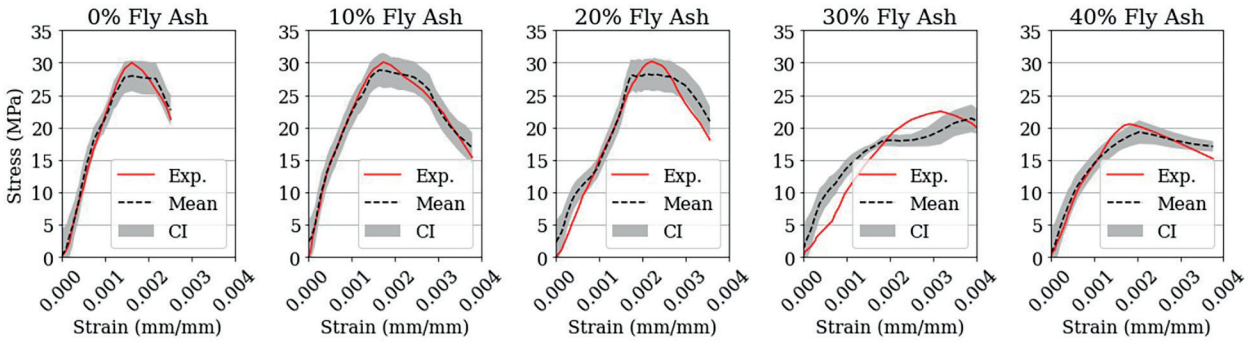

Fig. 15 Prediction results of concrete stress-strain curve obtained by Dropout-NN model

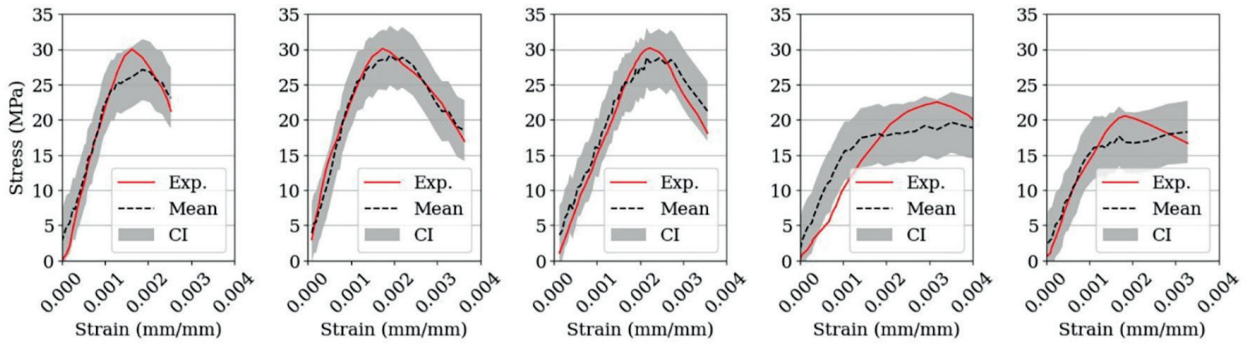

Fig. 16 Prediction results of concrete stress-strain curve obtained by Bayesian-NN model

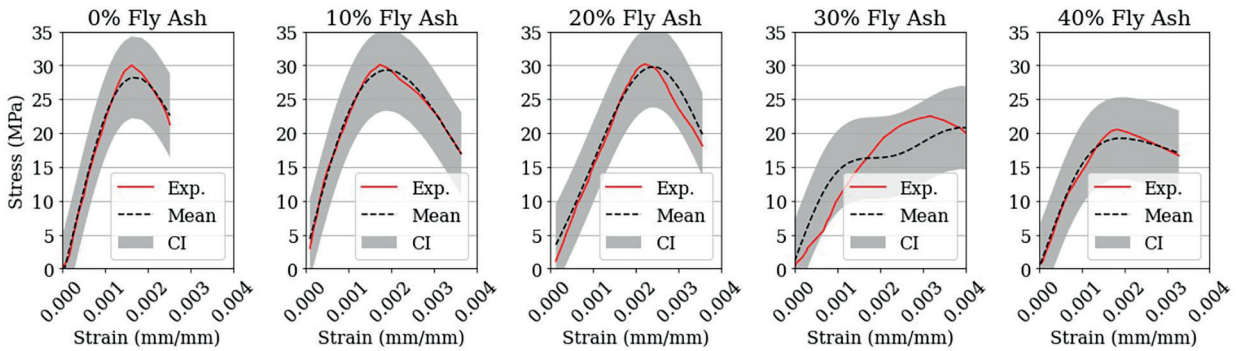

Fig. 17 Prediction results of fly ash concrete stress-strain curve obtained by GP model

and Bayesian-NN models to some extent. In terms of time complexity, the Bayesian-NN model takes nearly two and three-fold the training time compared to the Dropout-NN and GP models, respectively. Therefore, the selected Dropout-based model has the best balance between performance and time complexity.

5 Conclusions

Based on the experimental data obtained and the probabilistic investigation using three artificial intelligence-based models proposed in this study, a number of conclusions can be withdrawn as follows:

- It is feasible to produce fly ash concrete (FAC) with a mean cylinder compressive strength of about 30 MPa in laboratory conditions utilizing fly ash taken from Hongsa thermal power plant, Lao DPR. This is an encouragement for further studies and applications of sustainable construction materials from new fly ash sources in this Asian developing country;
- It is experimentally proved that compared to the other investigated dosages of fly ash, the by-mass 20% of ordinary Portland cement (OPC) to be replaced by fly ash (FA) is the most efficient percentage since the obtained FAC not only performed better workability with higher slump and lower water lost due to the hydration reaction, but also gained the highest 28-day compressive strength and tensile split strength as well as the most favorable development of compressive strength;
- In this study, three probabilistic models including Dropout Neural Network (Dropout-NN), Bayesian Neural Network (Bayesian-NN) and Gaussian Process (GP) are adopted and compared to other 27 machine learning models from the literature (that were mostly conducted in a deterministic manner) with relatively good results in terms of statistical metric R^2, which are 0.92, 0.90 and 0.88, respectively. This sets a basis to promote the proposed probabilistic models for further investigation.
- The predictions obtained from the proposed probabilistic models include not only the compressive strength as a point estimation but also the whole stress-strain curve associated with the corresponding uncertainty quantification in terms of (5%, 95%) confidence interval. It is shown from the probabilistic investigations that the FA/OPC replacement percentage of 20% is also the most effective value for FAC.
- It is proved in this study that among the proposed models, Dropout-NN is the model having the best balance between performance and time complexity.

Although the nature of fly ash can vary from region to region, the eventual optimum FA replacement may not be the same, but the presented methodology can be adjusted straightforwardly and provide desirable results. Additionally, the experimental results can enrich the fly ash concrete database in Asia countries. On the other hand, artificial intelligence probabilistic models can also be used as benchmarks for future studies.

In order to reduce the considerable uncertainties observed from the investigations on concrete presented in this study, a possible way is to take into account the process factors such as type of curing, humidity, environmental temperature, etc. By doing so, the proposed model can be extended to on-site samples which involve uncontrolled process factors. Another aspect to improve in the next study is to upgrade the proposed models into an automated framework which includes a variety of machine learning and deep learning models and a friendly input/output interface, helping structural engineers spend more time on the analysis of the concrete properties with less time on coding or learning algorithms.

Acknowledgement

The project presented in this article is supported by Hanoi University of Civil Engineering (HUCE), under grant number 44-2021/KHXD-TD. The authors' appreciation is also given to technicians of LAS-XD 125 (HUCE) for their sufficient supports during the materials tests.

References

[1] ACI "ACI PRC-232.2-18: Report on the Use of Fly Ash in Concrete", American Concrete Institute, Farmington Hills, MI, USA, 2018.

[2] Gołaszewski, J., Ponikiewski, T., Kostrzanowska-Siedlarz, A., Miera, P. "Technological Aspects of Usage of Calcareous Fly Ash as a Main Constituent of Cements", Periodica Polytechnica Civil Engineering, 65(2), pp. 619–637, 2021. https://doi.org/10.3311/PPci.11164

[3] ASTM "ASTM C618-12a Standard specification for coal fly ash and raw or calcined natural Pozzolan for use in concrete", ASTM International, West Conshohocken, PA, USA, 2015. https://doi.org/10.1520/C0618-12A

[4] Kaveh, A., Khalegi, A. "Prediction of strength for concrete specimens using artificial neural networks", In: Proceedings of the 1st International Conference on Engineering Computational Technology / 4th International Conference on Computational Structures Technology, Edinbourgh, Scotland, 1998, pp. 165–171. ISBN 0-948749-55-5

[5] Chindaprasirt, P., Jaturapitakkul, C., Chalee, W., Rattanasak, U. "Comparative study on the characteristics of fly ash and bottom ash geopolymers", Waste Management, 29, pp. 539–543, 2009. https://doi.org/10.1016/j.wasman.2008.06.023

[6] Marthong, C., Agrawal T. P. "Effect of fly ash additive on concrete properties", International Journal of Engineering Research and Applications, 2(4), pp. 1986–1991, 2012.

[7] Kao, Y.-C., Chiu, C.-K., Ueda, T., Juan, Y.-J. "Experimental investigation on mechanical properties of SBR - Modified mortar with fly ash for patch repair material", Journal of Advanced Concrete Technology, 16(8), pp. 382–395, 2018. https://doi.org/10.3151/jact.16.382

[8] Srinivasa Reddy, V., Seshagiri Rao, M. V., Shrihari, S. "Strength conversion factors for concrete based on specimen geometry, aggregate size and direction of loading", International Journal of Recent Technology and Engineering, 8(2), pp. 2125–2130, 2019. https://doi.org/10.35940/ijrte.B2336.078219

[9] Salla, S. R., Modhera, C. D., Babu, U. R. "An experimental study on various industrial wastes in concrete for sustainable construction", Journal of Advanced Concrete Technology, 19, pp. 133–148, 2021. https://doi.org/10.3151/jact.19.133

[10] Lizarazo-Marriaga, J., Higuera, C., Guzmán, I., Fonseca, L. "Probabilistic modeling to predict fly-ash concrete corrosion initiation", Journal of Building Engineering, 30, 101296, 2020. https://doi.org/10.1016/j.jobe.2020.101296

[11] Kandiri, A., Sartipi, F., Kioumarsi, M. "Predicting compressive strength of concrete containing recycled aggregate using modified ANN with different optimization algorithms", Journal of Applied Sciences, 11(2), 485, 2021. https://doi.org/10.3390/app11020485

[12] Tenza-Abril, A. J., Villacampa, Y., Solak, A. M., Baeza-Brotons, F. "Prediction and sensitivity analysis of compressive strength in segregated lightweight concrete based on artificial neural network using ultrasonic pulse velocity", Construction and Building Materials, 189, pp. 1173–1183, 2018. https://doi.org/10.1016/j.conbuildmat.2018.09.096

[13] Young, B. A., Hall, A., Pilon, L., Gupta, P., Sant, G. "Can the compressive strength of concrete be estimated from knowledge of the mixture proportions?: New insights from statistical analysis and machine learning methods", Cement and Concrete Research, 115, pp. 379–388, 2019. https://doi.org/10.1016/j.cemconres.2018.09.006

[14] Nguyen, T. T., Ngoc, L. T., Vu, H. H., Thanh, T. P. "Machine learning-based model for predicting concrete compressive strength", International Journal of GEOMATE, 20(77), pp. 197–204, 2021. https://doi.org/10.21660/2020.77.j2019

[15] Tahwia, A. M., Heniegal, A., Elgamal, M. S., Tayeh, B. A."The prediction of compressive strength and non-destructive tests of sustainable concrete by using artificial neural networks", Computers and Concrete, 27(1), pp. 21–28, 2021. https://doi.org/10.12989/cac.2021.27.1.021

[16] Dutta, S., Samui, P., Kim, D. "Comparison of machine learning techniques to predict compressive strength of concrete", Computers and Concrete, 21(4), pp. 463–470, 2018. https://doi.org/10.12989/cac.2018.21.4.463

[17] Kaveh, A., Bakhshpoori, T., Hamze-Ziabari, S. M. "M5' and Mars based prediction models for properties of self-compacting concrete containing fly ash", Periodica Polytechnica Civil Engineering, 62(2), pp. 281–294, 2018. https://doi.org/10.3311/PPci.10799

[18] Ahmad, A., Ahmad, W., Aslam, F., Joyklad, P. "Compressive strength prediction of fly ash-based geopolymer concrete via advanced machine learning techniques", Case Studies in Construction Materials, 16, e00840, 2022. https://doi.org/10.1016/j.cscm.2021.e00840

[19] Amin, M. N., Khan, K., Javed, M. F., Aslam, F., Qadir, M. G., Faraz, M. I. "Prediction of mechanical properties of fly-ash/slag-based geopolymer concrete using ensemble and non-ensemble machine-learning techniques", Materials, 15(10), 3478, 2022. https://doi.org/10.3390/ma15103478

[20] Khursheed, S., Jagan, J., Samui, P., Kumar, S. "Compressive strength prediction of fly ash concrete by using machine learning techniques", Innovative Infrastructure Solutions, 6, 149, 2021. https://doi.org/10.1007/s41062-021-00506-z

[21] Ahmed, A. H. A., Jin, W., Ali, M. A. H. "Artificial intelligence models for predicting mechanical properties of recycled aggregate concrete (RAC): Critical review", Journal of Advanced Concrete Technology, 20(6), pp. 404–429, 2022. https://doi.org/10.3151/jact.20.404

[22] Kaveh, A., Gholipour, Y., Rahami, H. "Optimal design of transmission towers using genetic algorithm and neural networks", International Journal of Space Structures, 23(1), pp. 1–19, 2008. https://doi.org/10.1260/026635108785342073

[23] Rofooei, F. R., Kaveh, A., Farahani, F. M. "Estimating the vulnerability of the concrete moment resisting frame structures using artificial neural networks", International Journal of Optimization in Civil Engineering, 1(3), pp. 433–448, 2011. [online] Available at: http://ijoce.iust.ac.ir/article-1-49-en.html

[24] Kaveh, A., Elmieh, R., Servati, H. "Prediction of moment-rotation characteristic for semi-rigid connections using BP neural networks", Asian Journal of Civil Engineering 2(2), pp. 131–142, 2001.

[25] Kaveh, A., Iranmanesh, A. "Comparative study of backpropagation and improved counterpropagation neural nets in structural analysis and optimization", International Journal of Space Structures, 13(4), pp. 177–185, 1998. https://doi.org/10.1177/026635119801300401

[26] Kaveh, A., Servati, H. "Design of double layer grids using back-propagation neural networks", Computers & Structures, 79(17), pp. 1561–1568, 2001. https://doi.org/10.1016/S0045-7949(01)00034-7

[27] Yeh, I.-C. "Modeling of strength of high-performance concrete using artificial neural networks", Cement and Concrete Research, 28(12), pp. 1797–1808, 1998. https://doi.org/10.1016/S0008-8846(98)00165-3

[28] Sevim, U. K., Bilgic, H. H., Cansiz, O. F., Ozturk, M., Atis, C. D. "Compressive strength prediction models for cementitious composites with fly ash using machine learning techniques", Construction and Building Materials, 271, 121584, 2021. https://doi.org/10.1016/j.conbuildmat.2020.121584

[29] Huang, J., Sun, Y., Zhang, J. "Reduction of computational error by optimizing SVR kernel coefficients to simulate concrete compressive strength through the use of a human learning optimization algorithm", Engineering with Computers, 2021. https://doi.org/10.1007/s00366-021-01305-x

[30] Farooq, F., Ahmed, W., Akbar, A., Aslam, F., Alyousef, R. "Predictive modeling for sustainable high-performance concrete from industrial wastes: A comparison and optimization of models using ensemble learners", Journal of Cleaner Production, 292, 126032, 2021. https://doi.org/10.1016/j.jclepro.2021.126032

[31] ASTM "ASTM C150/C150M-20 Standard specification for Portland cement", ASTM International, West Conshohocken, PA, USA, 2020. https://doi.org/10.1520/C0150_C0150M-20

[32] Nidonekeo, B., Salackchit, P. "Management of fly ash business", Report of Fly Ash Business Division, Lao Holding State Enterprise, Vientiane, Laos, 2019.

[33] ASTM "ASTM C33/C33M-18 Standard specification for concrete aggregates", ASTM International, West Conshohocken, PA, USA, 2018. https://doi.org/10.1520/C0033_C0033M-18

[34] TCVN "TCVN 10303:2014 Concrete - Control and assessment of compressive strength", Vietnam Ministry of Science and Technology, Hanoi, Vietnam, 2018.

[35] ASTM "ASTM C39/C39M-2 Standard test method for compressive strength of cylindrical concrete specimens", ASTM International, West Conshohocken, PA, USA, 2020. https://doi.org/10.1520/C0039_C0039M-21

[36] ASTM "ASTM C469/c469m-14 Standard test method for static modulus of elasticity and Poisson's ratio of concrete in compression", ASTM International, West Conshohocken, PA, USA, 2014. https://doi.org/10.1520/C0469_C0469M-14

[37] Gal, Y., Ghahramani, Z. "Dropout as a Bayesian approximation: Representing model uncertainty in deep learning", In: Proceedings of the 33rd International Conference on Machine Learning, New York, NY, USA, 2018, pp. 1050–1059.

[38] Orre, R., Lansner, A., Bate, A., Lindquist, M. "Bayesian neural networks with confidence estimations applied to data mining", Computational Statistics and Data Analysis, 34(4), pp. 473–493, 2020. https://doi.org/10.1016/S0167-9473(99)00114-0

[39] Rasmussen, C. E., Williams, C. "Gaussian Processes for Machine Learning", MIT Press, 2006. ISBN 026218253X

[40] Srivastava, N., Hinton, G., Krizhevsky, A., Sutskever, I., Salakhutdinov, R. "Dropout: a simple way to prevent neural networks from overfitting", Journal of Machine Learning Research, 15, 1929–1958, 2014. [online] Available at: https://jmlr.org/papers/v15/srivastava14a.html

[41] Paszke, A., Gross, S., Massa, F., Lerer, A., Bradbury, J., … , Chintala, S. "Pytorch: An imperative style, high-performance deep learning library", In: Advances in Neural Information Processing Systems, Proceedings of the 32rd Conference on Neural Information Processing Systems, Vancouver, Canada, 2019, pp. 8024–8035. ISBN: 9781713807933 https://doi.org/10.48550/arXiv.1912.01703

[42] Bingham, E., Chen, J. P., Jankowiak, M., Obermeyer, F., Pradhan, N., Karaletsos, T., Singh, R., Szerlip, P., Horsfall, P., Goodman, N. D. "Pyro: Deep universal probabilistic programming", Journal of Machine Learning Research, 20, pp. 973–978, 2019. [online] Available at: http://jmlr.org/papers/v20/18-403.html

[43] Gardner, J. R., Pleiss, G., Bindel, D., Weinberger, K. Q., Wilson, A. G. "Gpytorch: Blackbox matrix-matrix Gaussian process inference with GPU acceleration", In: Advances in Neural Information Processing Systems, Proceedings of the 31rd Conference on Neural Information Processing Systems, Montréal, Canada, 2019, pp. 7587-7597. ISBN: 9781510884472 https://doi.org/10.48550/arXiv.1809.11165

[44] Akiba, T., Sano, S., Yanase, T., Ohta, T., Koyama, M. "Optuna: A next-generation hyperparameter optimization framework", In: Proceedings of the 25th ACM SIGKDD International Conference on Knowledge Discovery & Data Mining, Anchorage, AK, USA, 2019, pp. 2623–2631. ISBN 978-1-4503-6201-6 https://doi.org/10.1145/3292500.3330701